Assessing the Efficacy of Pixel-based and Object-based Classification Techniques and Classifiers for Land Cover Mapping Using Landsat-8 and Sentinel-2 Data in Complex Mountainous Terrain

Mati ur Rehman[1], Syed Aun Abbas[1], Abdul Wahab Shah[1], Raja Tashfeen Muqarrab[1], Dur E Najaf Raza[1], Sawaid Abbas[1,2*]

[1]Smart Sensing for Climate and Development, Center for Geographical Information System, University of the Punjab, Lahore, Pakistan

[2]Department of Land Surveying and Geo-Informatics, The Hong Kong Polytechnic University, Hong Kong SAR

***Correspondence**: sawaid.gis@pu.edu.pk (S.A); sawaid.abbas@connect.polyu.hk

Citation | Rehman. M. U, Abbas. S. A, Shah. A. W, Muqarrab. R. T, Raza. D. N, Abbas. S, "Assessing the Efficacy of Pixel-based and Object-based Classification Techniques and Classifiers for Land Cover Mapping Using Landsat-8 and Sentinel-2 Data in Complex Mountainous Terrain", IJIST, Vol. 07 Special Issue. pp 42-56, July 2025

Received | July 11, 2025 **Revised |** July 24, 2025 **Accepted |** July 29, 2025 **Published |** July 31, 2025.

Disaster mitigation and climate-resilient planning heavily depend on accurate Land Use and Land Cover (LULC) datasets. Well-classified LULC data optimizes hazard modeling, surface runoff estimation, and sustainable land use planning, enabling informed decision-making and proactive risk reduction. However, supervised LULC classification faces challenges such as selecting optimal Machine Learning (ML) algorithms, differences in spatial and spectral resolution, and seasonal variability. This study adopts a multi-tiered approach to generate effective LULC maps for Gilgit District, Pakistan, by comparing pixel-based classification and object-based image analysis (OBIA) methods. Pixel-based classification was performed on Google Earth Engine (GEE) using Landsat-8 and Sentinel-2 imagery, applying three classifiers: Random Forest (RF), Support Vector Machine (SVM), and k-Nearest Neighbor (k-NN). OBIA involved multi-resolution segmentation, followed by training and classification on image objects using the same algorithms. Validation using independent samples revealed that object-based maps were visually smoother and more realistic. Quantitatively, pixel-based RF yielded the highest accuracy: 82.9% for Landsat-8 and 78.02% for Sentinel-2. In contrast, OBIA k-NN achieved superior accuracy: 81.3% on Landsat-8 and 83.6% on Sentinel-2. Remaining classifiers also provided nearby results in both classification methods. Lower accuracy in Sentinel-2 may be due to within-class spectral variability at 10m spatial resolution, while Landsat-8's lower resolution (30m) reduced object-based segmentation performance, resulting in object heterogeneity and misclassification. Although pixel-based classification provided promising results, OBIA ultimately demonstrated superior overall accuracy. This study highlights the importance of resolution-context compatibility and algorithm choice in enhancing LULC classification, which is essential for reliable climate-responsive planning, disaster preparedness, and sustainable development.

Keywords: LULC; Machine Learning; OBIA vs Pixel-based; Gilgit; GEE

Introduction:

During the early 21st century, the increase in global population and unmanaged economic development have significantly triggered changes in LULC. Quantitative assessment of LULC changes is one of the most effective approaches for evaluating and managing land transformation [1]. Land surface mapping is a commonly used environmental monitoring technique that plays a vital role in studying the impacts of climate change [2]. Knowledge of LULC is crucial for effective disaster risk reduction and the sustainable management of land and water resources [3][4]. Its consistent analysis is essential in interpreting global phenomena such as drought, flooding, urbanization, and deforestation [5]. Detailed information on various land cover types is necessary to develop effective policies [6]. The availability of open-access satellite data has facilitated the timely generation of LULC maps, leading to a growing demand for up-to-date land cover information [7].

Remote sensing is one of the techniques, extensively employed for land cover mapping and monitoring its transformations over time [8]. Compared to traditional ground-based methods, remote sensing is convenient, efficient, time-saving, and cost-effective [9]. Optical Remote Sensing (ORS) is frequently used for land observation, providing a variety of data with diverse spatial, spectral, and temporal resolutions. Landsat-8 and Sentinel-2 imagery are among the widely utilized sources in the low- to medium-resolution satellite category [10]. They are widely used globally due to their free accessibility of imagery and their spatial and spectral resolutions, which enable the generation of valuable results [11], transforming raw satellite imagery into meaningful information, and their interpretation is achieved by image classification [12]. It is pivotal in generating LULC thematic maps that support sustainable land use by balancing development and environmental conservation [13]. The first challenge in this scenario is to determine the most suitable method for classification. There are two approaches most commonly used for image classification: the classical Pixel-based and OBIA approaches [12][14][9]. The pixel-based classification depends only on the spectral information of the pixel, while the object-based classification utilizes spectral and spatial features [12]. Pixel-based classification methods analyze individual pixels, which often struggle with increased variability, leading to spectral mixing and lower accuracies [15]. In comparison, OBIA represents a methodological shift from traditional pixel-based classification approaches by interpreting images through meaningful objects and their spatial relationships, rather than individual pixels. It incorporates statistical descriptors such as mean, standard deviation, and mode, which enhance the differentiation between land cover classes [12]. Beyond these frameworks, ML algorithms have gained popularity for classifying land cover [16].These classifiers can be integrated into both workflows, but selecting the appropriate ML algorithm remains challenging, making it essential to evaluate the accuracy of different classifiers for their practical application, especially in a mountainous landscape [17].

Creating accurate land cover maps involves significant challenges in image classification, and we must choose an efficient approach with a suitable ML algorithm for precise map classification [12]. Based on literature review, we selected the most popular ML classifiers like SVM, which is suitable for handling complex data and offers high accuracy in land cover classification, especially with multisource inputs [18], RF, which handles high-dimensional data, its fast performance and high accuracy making it a popular choice [12], k-NN which is a simple, non-parametric classification method known for its effectiveness, though it can be computationally intensive during prediction [19]. Many studies have used these classifiers for LULC mapping [14][5][20][17][9][21][16][19], and according to [22], RF, SVM, and k-NN are three prominent classifiers recognized for producing high accuracies. Mapping over a vast area encounters many challenges, primarily due to the extensive data involved, and managing these datasets requires a lot of storage and processing power to achieve fast and precise results [23]. The advent of Google Earth Engine (GEE) has addressed this challenge by integrating remote sensing with big data, providing a cloud-based, high-performance platform for efficient processing and analysis [24].

To identify the effective method and high-performing ML algorithm for accurate classification, we delineate a comparison of both pixel-based and OBIA approaches and the performance of SVM, RF, and k-NN classifiers on Landsat-8 and Sentinel-2 imagery of Gilgit District, Pakistan. There is limited research on assessing ML classifiers and classification methods within a single study. Existing studies, especially those for this and the nearby region, focus primarily on the assessment of ML algorithms.[16]. The novelty of this study is that we compare the two popular classification techniques (pixel-based and OBIA) with the comparative assessment of three ML classifiers using multi-scale imagery. The literature gap highlights the need for a comprehensive comparative study of classification methods and classifiers using multi-spatial and spectral datasets, particularly in this complex terrain.

Novelty:

The three objectives of this study are; (1) to determine the applicability of pixel-based classification and OBIA methods, (2) investigate the performance of three ML classifiers (SVM, RF, k-NN) for accurate LULC mapping, and (3) assessing the impact of varying spatial and spectral resolutions (30 m of Landsat-08 and 10m of Sentinel-2 imageries) on accuracy of LULC classification. This evaluation would provide valuable guidance on selecting the optimal approach, identifying the best-performing classifier, and assessing the compatibility of datasets with resolution context for reliable image classification, ultimately supporting climate-responsive planning, sustainable land management, and disaster preparedness. The remaining paper is structured as follows: Section-2 presents the overall experimental design, including materials and methods. The experiment results related to the objectives and discussions are listed in Section-3, and the conclusion, including the significance and limitations of the study, is summarized in Section-4.

Materials & Methods:

Study Area:

Gilgit District is situated in Gilgit-Baltistan (GB), a province in Pakistan. This is a region home to some of the world's highest mountain ranges, including the Karakoram [25]. Gilgit District is the administrative capital of GB and has geographical coordinates of 35.8819° N to 74.4643° E [26]. It spans approximately 40,8100 hectares (ha) of area bordered by Shigar and Skardu districts to the east, Diamer and Astore to the south, Ghizer to the west, and Nagar to the north. Its average annual temperature is about 2.59 °C, average summer temperature is 14.09°C, and -8.94°C average temperature in winters [27]. This district has significant environmental, geographical, and socio-economic importance. It is in the buffer zone to the route of China–Pakistan Economic Corridor (CPEC), a popular tourist spot and prone to natural disasters [26][25][16]. This highlights the need for accurate LULC mapping for disaster management and urban planning, which aligns with the aims of this study. Figure 1. provides the graphical layout of the study area.

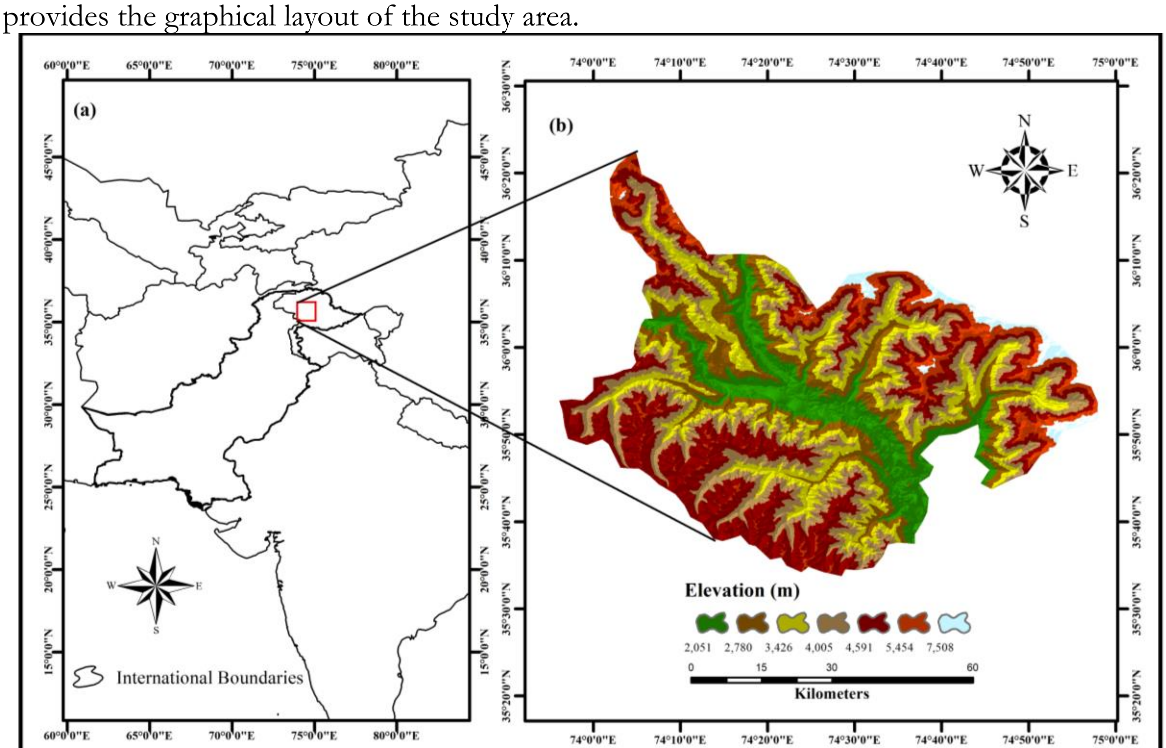

Figure 1. Location of study area **(a)** International Boundaries **(b)** Location of the study area with elevation derived from Shuttle Radar Topography Mission (SRTM) (30 m) data

Data Collection:

Landsat-8, launched on February 11, 2013, by the National Aeronautics and Space Administration (NASA) in partnership with the U.S. Geological Survey (USGS), carries the Operational Land Imager (OLI), which measures visible, near infrared (NIR), and shortwave infrared (SWIR) portions of the electromagnetic spectrum. Landsat-8 images have 30-meter multispectral spatial resolutions (as outlined in Table 1) and a 16-day temporal resolution. Landsat-8 surface reflectance products are generated using the Land Surface Reflectance Code (LaSRC) algorithm [28]. In the GEE catalog, OLI data is available as USGS Landsat-8 Level 2, Collection 2 product, which can be accessed using code 'ee.ImageCollection("LANDSAT/LC08/C02/T1_L2")' [29].

Sentinel-2A was launched on June 23, 2015, by the European Space Agency (ESA) as part of the Copernicus program. It has a 10-meter spatial resolution with 13 spectral bands for specialized coverage of land and vegetation, ranging from visible to SWIR wavelengths of the spectrum (displayed in Table 1). It has a 5-day revisit time and a swath of 290 km, providing frequent land cover images [30]. Sentinel-2 Multispectral Instrument (MSI) data is available as Level-2A Surface Reflectance (SR) product in GEE, and it can be retrieved by using code 'ee.ImageCollection("COPERNICUS/S2_SR")' [31].

Table 1. Description of datasets used in this study

Satellite Sensors	*Bands Used*	*Description*	*Wavelength (µm)*	*Spatial Resolution(m)*	*Date of Acquisition*
Landsat-8 OLI Surface Reflectance Tier-2	B2	Blue	0.450 - 0.51	30	12-September-2024 and 21-September-2024
	B3	Green	0.53-0.59	30	
	B4	Red	0.64 - 0.67	30	
	B5	NIR	0.85 - 0.88	30	
	B6	SWIR-I	1.57 - 1.65	30	
	B7	SWIR-II	2.11 - 2.29	30	
Sentinel-2 MSI-Level 2A (SR)	B2	Blue	0.4966	10	21-September-2024
	B3	Green	0.560	10	
	B4	Red	0.6645	10	
	B8	NIR	0.8351	10	
	B11	SWIR-I	1.6137	20	
	B12	SWIR-II	2.2024	20	

A brief overview of methodology:

The methodology in this study involves the acquisition of Landsat-8 OLI SR level 2 imagery for September 12 and 21, 2024, as the study area was covered in two tiles. Sentinel-2 MSI Level 2A imagery for September 21, 2024, with cloud cover less than 7% for both images, was selected. The month of September was chosen to avoid the impact of monsoon rains and the fresh snow on classification results. Then, the image preprocessing and Landsat-8 imagery mosaic were performed in GEE. Seven classes were defined based on the literature review [16][17][11][27], illustrated in Table 2.

The training samples were collected and independent validation samples were employed for training of the classifiers and for validation purposes, distributed evenly across the study area. The samples for land cover classes were visually interpreted from high-resolution Google Earth Pro imagery. Additionally, ML classifiers, RF, SVM, and k-NN, were applied for pixel-based classification, without any hyperparameter tuning. The accuracy assessment was done on the classified rasters to evaluate the performance of classifiers. The validation samples were collected independently to ensure the reliability, consistency, and unbiased accuracy assessment of the classification. OBIA was performed in e-Cognition Developer. Initially, segmentation was carried out using a multiresolution segment with a shape factor of 0.1, compactness of 0.4, and a scale parameter of 50 for Sentinel-2 and 70 for Landsat-8. This was due to the 30-meter spatial resolution of Landsat-8, which led to difficulty in accurately delineating small and heterogeneous land cover features. The model was subsequently trained using the three classifiers, and they were then applied sequentially to obtain the classified outputs. Accuracy assessment was performed on the resulting rasters using standard metrics including Overall accuracy (OA), User's accuracy (UA), Producer's accuracy (PA), and Kappa Coefficient. The flow of this study is provided in Figure 2.

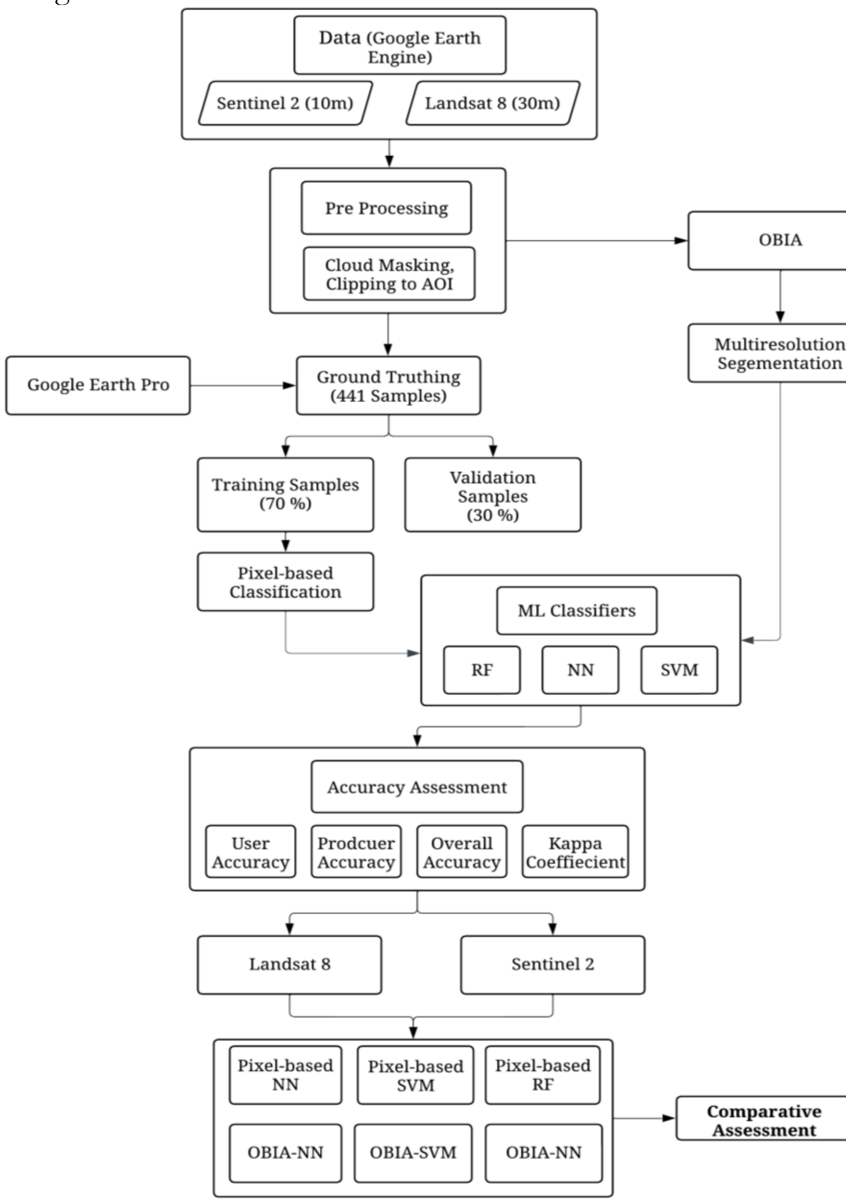

Figure 2. Flowchart of Study

Table 2. Land Cover classes were delineated based on the literature review

Classes	**Description**
Rock / Soil	Land areas of exposed soil and bare mountains
Grass / Shrub	Grasses, grass-like plants, forbs, or shrubs
Forest	Dense vegetation, mixed forest, and Tree cover
Cropland	Arable, horticultural, and ploughed land
Built-up Area	Urban and rural settlements
Snow / Glacier	Clean ice and debris
Water	Shallow water, rivers, and natural lakes

Machine Learning Algorithms:

Random Forest:

Random Forest (RF) is also a binary decision tree that utilizes multiple independent decision trees to facilitate classification. It builds numerous randomized decisions trees and utilizes predictions from the previously constructed trees. A subset of the input data is used for training, and the remaining data is for unbiased validation. The final classification decision is made by calculating the mean of the class probability estimates across all the single trees. RF is considered to have high stability and be tolerant to overfitting and noise due to the nature of the algorithm, and it is also suitable for high-dimensional datasets [21]. The performance of RF depends on several parameters, and the number of trees and the number of variables at each node are critical, which were set to 100 in this study [5]. The *'classifier.smileRandomForest'* function within the Google Earth Engine (GEE) library was utilized to implement RF classification.

Support Vector Machine:

Initially, SVM was created for separating classifications using Structural Risk Minimization (SRM). The Support Vector Machine (SVM) utilizes a hyperplane to separate data points by maximizing the distance between classes through support vectors, effectively handling both categorical variables and linear as well as non-linear datasets. Radial Basis Function (RBF) and polynomial kernels are commonly utilized in sensing applications; however, RBF is preferred for LULC categorization due to its proven level of accuracy. The process of SVM classification involves finding the decision boundary using a kernel function to reduce errors and create clear decision boundaries effectively [18]. Choosing the kernel greatly influences how smooth the separation surface is, for multispectral data where performance can be improved by carefully selecting a suitable kernel and possibly fine-tuning it with genetic optimization techniques aimed at defining a boundary that maximizes the distance between support vectors, for accurate classification purposes [5]. This study employed the *'classifier.libsvm'* method from the Google Earth Engine (GEE) library, using the RBF kernel type, a Gamma value of 10, and a Cost value of 20 for SVM classification implementation.

K-Nearest Neighbor:

K-Nearest Neighbor (k-NN) is a fundamental, straightforward classification method, beneficial when the data distribution is unknown [14]. As a 'lazy learning' algorithm, it stores all training data and classifies new samples by identifying their K nearest neighbors. The latest sample's class is then determined by voting or weighted sums among these neighbors. Neighbors are identified by calculating distances between the input vector and all training samples, then ordering them by proximity [19][20]. Code snippet to access the k-NN *'ee.Classifier.smileKNN(k)'* was used in this study.

Classification Methods:

Pixel-based Classification:

Pixel-based supervised image classification is a traditional approach that assigns land cover classes by comparing the spectral signature of each pixel—represented as an n-dimensional data vector—to predefined class models. These spectral vectors typically consist of digital numbers (DN) values from multispectral bands [14]. This approach ignores contextual, spatial, and textural details in favor of relying only on the spectral information of each pixel. Because each pixel in high- or very high-spatial-resolution (VHSR) imagery may represent complex and varied surface features, it loses some of its dependability. The high intra-class variability and reduced inter-class separability at such resolutions often lead to reduced classification accuracy and the well-known "salt and pepper" noise [8]. Moreover, because image pixels do not represent actual geographical objects and lack topological relationships, the approach struggles to extract meaningful object-based insights. Despite this, pixel-based classification is widely appreciated for its simplicity, ease of implementation, and strong spectral discrimination capabilities, making it especially effective for moderate-resolution imagery where spectral variation between classes is distinct and sufficient for accurate land cover mapping. It is essential to consider the spatial and spectral resolution of the dataset, as the effectiveness of pixel-based classification largely depends on these parameters. That is why we assess the effectiveness of the pixel-based approach by comparing datasets with varying resolutions and analysis scales.

Object-based Image Analysis (OBIA):

Object-Based Image Analysis (OBIA) is a strong alternative to traditional pixel-based methods because it uses not only spectral information but also spatial, textural, and contextual attributes of image data. OBIA groups neighboring pixels into meaningful image objects through segmentation, which is a key step in the classification process. These image objects, characterized by homogeneity in shape, size, texture, and spectral properties, are then classified based on a combination of their features [12]. The segmentation process typically follows a bottom-up principle, where small segments are progressively merged based on homogeneity criteria such as scale, spectral similarity, and spatial characteristics, commonly using multi-resolution region-growing techniques [15]. This approach enables OBIA to more accurately represent real-world features and mitigate classification noise, such as the "salt-and-pepper" effect commonly found in pixel-based methods. Although threshold setting for segmentation parameters can influence outcomes—potentially causing over- or under-segmentation—OBIA's ability to integrate geometric and contextual information significantly enhances classification accuracy, especially for very high-resolution remote sensing imagery [32]. It is imperative to consider the spatial and spectral resolution of the dataset, as they primarily depend on these factors. In this study, we compare multi-resolution and multi-scale datasets to evaluate the efficiency of the object-based approach. By grouping spectrally and spatially similar pixels into objects, OBIA helps in overcoming the limitations of pixel-level analysis and enhances the full potential of modern remote sensing datasets.

Ground Truth Information:

Accurate ground truth information plays a pivotal role in training and validating classification models [33]. In this study, a total of 441 ground reference points were established across the study area. We used high-resolution images from Google Earth Pro to mark these reference points because it has better spatial detail, temporal coverage, and visual clarity, making them a reliable source for interpreting land cover. Out of the total samples, 318 were used for model training and 123 were set aside for validation only, to ensure an unbiased and statistically sound assessment of classification performance. The training samples were manually digitized and plotted using the GEE platform, which facilitated the easy distribution and representation of classes across different landscapes [24]. We carefully labeled the land cover classes based on visual interpretation techniques and checked them against temporal data to reduce uncertainty. The validation dataset was used to independently assess classification accuracy through standard performance metrics, ensuring the reliability of the classification outputs.

Accuracy Assessment:

Using common confusion matrix-derived metrics, such as Overall Accuracy (OA), Kappa Coefficient (Kc), Producer's Accuracy (PA), and User's Accuracy (UA) for every land cover class, the accuracy of the LULC classification results was evaluated. As a general indicator of classification performance, OA shows the percentage of correctly classified pixels of all reference pixels. By taking into consideration the potential for agreement to occur by chance, the Kc offers a more thorough assessment and a more sophisticated understanding of classification reliability [34]. While UA indicates the possibility that a pixel classified into a particular category represents that class in reality (ground-truth), PA shows the likelihood that a reference pixel has been correctly classified [35]. The dataset was divided into 70% training and 30% validation subsets using a stratified random sampling technique to ensure an accurate and objective assessment and to guarantee that each land cover class was fairly represented. The independent validation (testing) samples derived from this stratified approach were used to compute all accuracy metrics. These metrics were used to systematically evaluate and compare the performance of the three machine learning classifiers—RF, SVM, and k-NN—under both pixel-based and OBIA approaches. The comparative analysis based on OA and Kappa values facilitated the identification of the most effective classification method and algorithm combination for accurately mapping the land cover.

Results:

Comparison of ML classifiers:

SVM, RF, and k-NN were applied to Landsat-8 and Sentinel-2 imagery using two different classification approaches to evaluate the performance of classifiers. Results, illustrated in Figure 3, displays the overall accuracy (OA) and kappa coefficient (Kc) of each classifier in four different cases. When the ML classifiers were applied to Landsat-8 imagery using a pixel-based approach, RF outperformed SVM and k-NN by achieving 82.9% OA and 0.796 Kappa coefficient, while SVM obtained 81.3 % OA and a Kappa coefficient of 0.777, and k-NN achieved OA of 78.9% and 0.747 Kappa coefficient. In the case of Sentinel-2 imagery using a pixel-based approach, RF again performed well among other classifiers, achieving an OA of 78% and a kappa coefficient of 0.737, while SVM reached an OA of 76.4% with a kappa coefficient of 0.719, and k-NN achieved an OA of 72.4% and a kappa coefficient of 0.666. In the OBIA method, when classifiers were applied to Landsat-8 imagery, k-NN surpassed other classifiers by achieving 81.3% OA and a kappa coefficient of 0.777. RF and SVM achieved an OA of 73.2% and 77.2% with a kappa coefficient of 0.676 and 0.728, respectively. Using Sentinel-2 imagery, k-NN achieved the highest OA of 83.6% with a kappa coefficient of 0.80, whereas RF achieved 75.6% OA with a kappa coefficient of 0.711, and SVM gained 72.4% OA and a kappa coefficient of 0.665. The user and producer accuracies of the best-performing classifiers in each case are depicted in Table 3.

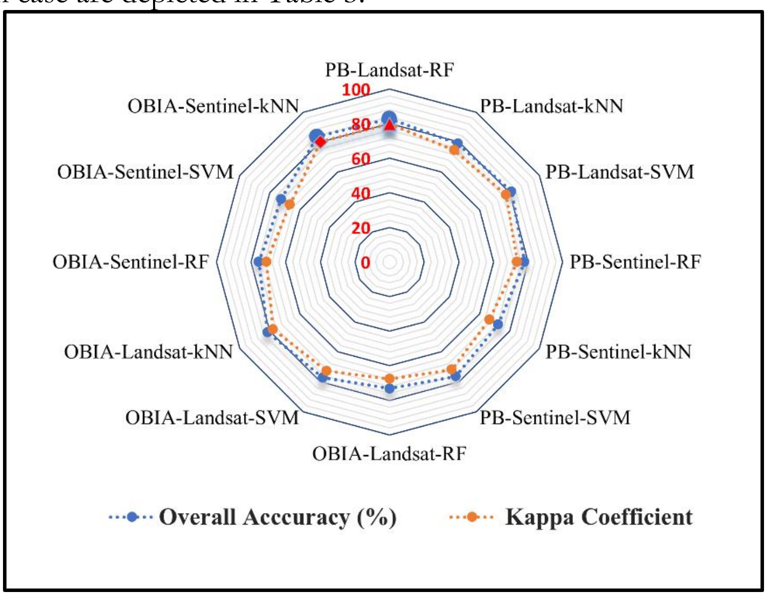

Figure 3. Overall accuracies and Kappa Coefficients of classification methods and classifiers

Pixel-based Classification using Landsat-8 imagery:

The SVM classifier identified 223,852 ha as rocky areas or bare land, 91,819 ha as shrubs or grasses, 13,654 ha as forest, 5,025 ha as cropland, 49,120 ha as snow, 11,520 ha as water bodies, and 13,110 ha as built-up and residential areas, using a pixel-based approach on Landsat-8 imagery. The RF classifier classified 217,825 ha as rock areas, 98,154 ha as grasses, 12,900 ha as forest, 6,039 ha as cropland, 13,900 ha as built-up areas, 48,200 ha as snow, and 11,082 ha as water bodies. The k-NN classifier observed 211,225 ha as bare areas, 108,000 ha as grasses, 11,990 ha as forest and tree cover, 5,636 ha as cropland, 14,289 ha as built-up areas, 47,100 ha as snow, and 9,860 ha as water bodies. The area statistics are also displayed in Figure 5.

The area under investigation was predominantly barren land, which was followed by land covered with grass and shrubs after the monsoon rains in September. The forest cover is typically found at high altitudes, as well as in dense and sparse tree cover in urban and rural settlements, residential areas, and cropland that lies along water bodies. It is distributed throughout the valleys, and snow covers the mountain-tops (glaciers), as there was no snowfall in September. Figure 4 illustrated the output rasters.

Table 3. Confusion matrices, UA, and PA of high-performing classifiers in both methods.

Land Cover	Rock / Soil	Grass / Shrub	Forest	Cropland	Built-up Area	Snow / Glacier	Water	PA
K-NN applied on Landsat-08 imagery using OBIA								
Rock / Soil	24	1	0	0	1	6	1	**82.75**
Grass / Shrub	4	14	0	0	0	2	1	**77.77**
Forest	0	3	19	0	0	0	0	**100**
Cropland	0	0	0	16	3	0	0	**100**
Built-up Area	0	0	0	0	10	0	0	**71.42**
Snow / Glacier	1	2	0	0	0	10	0	**55.55**
Water	0	0	0	0	0	0	7	**77.77**
UA	**72.72**	**66.66**	**86.36**	**84.21**	**100**	**90.9**	**100**	
K-NN applied on Sentinel-2 imagery using OBIA								
Rock / Soil	26	3	0	0	0	0	0	**78.78**
Grass / Shrub	0	16	0	1	0	1	0	**69.56**
Forest	0	0	14	2	0	0	0	**82.35**
Cropland	0	0	1	16	0	0	0	**88.88**
Built-up Area	1	0	0	0	13	0	0	**100**
Snow / Glacier	4	2	0	0	0	10	2	**90.9**
Water	0	1	0	0	0	0	8	**80**
UA	**89.65**	**88.88**	**73.68**	**100**	**92.86**	**55.55**	**88.88**	
RF applied on Landsat-08 imagery using a Pixel-based approach.								
Rock / Soil	24	4	0	0	2	4	0	**70.58**
Grass / Shrub	2	15	0	0	0	0	0	**68.18**
Forest	0	0	18	1	0	0	0	**94.73**
Cropland	0	0	0	16	1	0	0	**94.12**
Built-up Area	1	0	0	0	13	0	0	**100**
Snow / Glacier	5	3	0	0	0	9	1	**90**
Water	2	0	0	0	0	0	7	**87.5**
UA	**82.75**	**83.33**	**94.73**	**100**	**92.86**	**50**	**77.78**	
RF applied on Sentinel-2 imagery using a Pixel-based approach.								
Rock / Soil	26	3	0	0	0	0	0	**68.42**
Grass / Shrub	1	17	0	0	0	0	0	**65.38**
Forest	1	3	14	1	0	0	0	**87.5**
Cropland	0	0	2	14	0	0	0	**93.33**
Built-up Area	3	1	0	0	10	0	0	**90.9**
Snow / Glacier	6	2	0	0	1	9	0	**81.81**
Water	1	0	0	0	0	2	6	**100**
UA	**89.66**	**94.44**	**73.68**	**87.5**	**71.43**	**50**	**66.66**	

Pixel-based Classification using Sentinel-2 imagery:

The pixel-based method indicated that the RF classifier classified 201,115 ha as rock areas, 110,090 ha as grasses, 13,200 ha as forest, 5,137 ha as cropland, 15,100 ha as built-up areas, 53,300 ha as glacier or snow, and 10,158 ha as water bodies, using Sentinel-2 imagery. The k-NN classifier identified 220,010 ha as rock areas, 100,800 ha as shrubs or grasses, 12,070 ha as forest, 4,716 ha as cropland, 11,300 ha as built-up areas, 50,014 ha as snow, and 9,190 ha as water bodies, as depicted in Figure 5. SVM classifier detected 199,900 ha as rock areas, 119,010 ha as shrubs, 13,990 ha as forest, 4,100 ha as cropland, 48,102 ha as snow, and 12,084 ha as water bodies and built-up area as 10,914 ha. Figure 4 illustrates the resulting rasters.

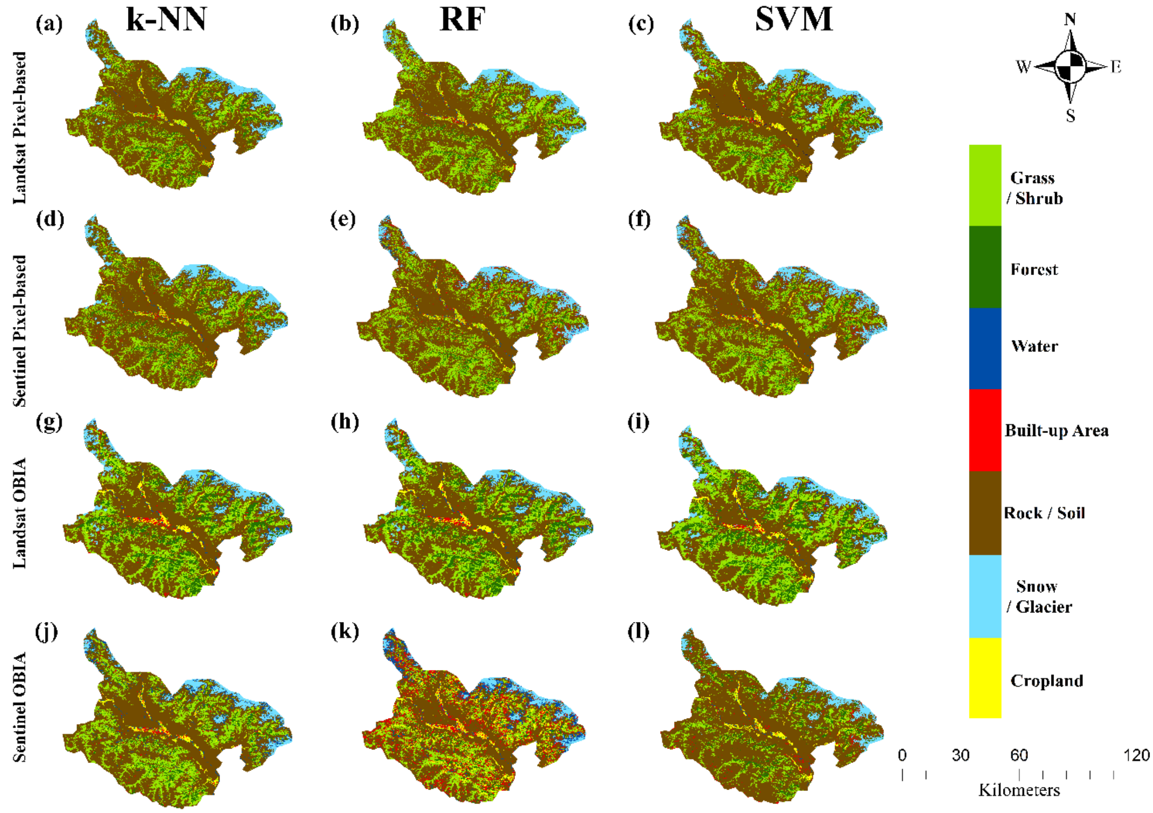

Figure 4. Spatial Distribution of LULC classification after applying RF, SVM, and k-NN on Landsat-8 and Sentinel-2 imagery using Pixel-Based and OBIA approach.

OBIA using Landsat-8 imagery:

The results obtained using the OBIA method on Landsat-8 imagery reveal that the RF classifier categorized 198,000 ha as rock areas, 130,400 ha as shrublands, 14,100 ha as forest, 5,850 ha as cropland, 12,100 ha as built-up areas, 48,900 ha as glaciers, and 8,950 ha as water bodies. The SVM classifier identified 225,825 ha as barren land, 89,029 ha as shrubland, 14,042 ha as forest, 6,320 ha as cropland, 13,010 ha as built-up areas, 50,520 ha as glaciers, and 9,354 ha as water bodies. The k-NN classifier classified 210,000 ha as rock areas, 101,010 ha as shrubs, 13,755 ha as forest, 7,510 ha as cropland, 14,500 ha as built-up areas, 49,990 ha as glacier, and 11,335 ha as water bodies. Figure 4 demonstrates the results, and Figure 5 presents the comparison of land cover area among the classifiers.

OBIA using Sentinel-2 imagery:

On Sentinel-2 imagery, OBIA exhibits that the RF classifier in the object-based approach using Sentinel-2 imagery identified 211,003 ha as rocky areas or bare land, 106,010 ha as grasses, 14,120 ha as forest, 5,452 ha as cropland, 51,113 ha as snow or glacier, 11,302 ha as water bodies, and 9,100 ha as built-up and residential areas. The SVM classifier identified 208,012 ha as rock areas, 111,001 ha as grasslands, 13,502 ha as forest, 6,120 ha as cropland, 12,300 ha as built-up areas, 47,233 ha as glaciers, and 9,932 ha as water bodies. The k-NN classifier observed 198,123 ha as bare areas, 121,100 ha as grasses, 12,600 ha as forest and tree cover, 5,863 ha as cropland, 10,100 ha as built-up areas, 50,013 ha as snow, and 10,301 ha as water bodies. Classified rasters are shown in Figure 4, and Figure 5 depicts the comparison of the area of each classifier.

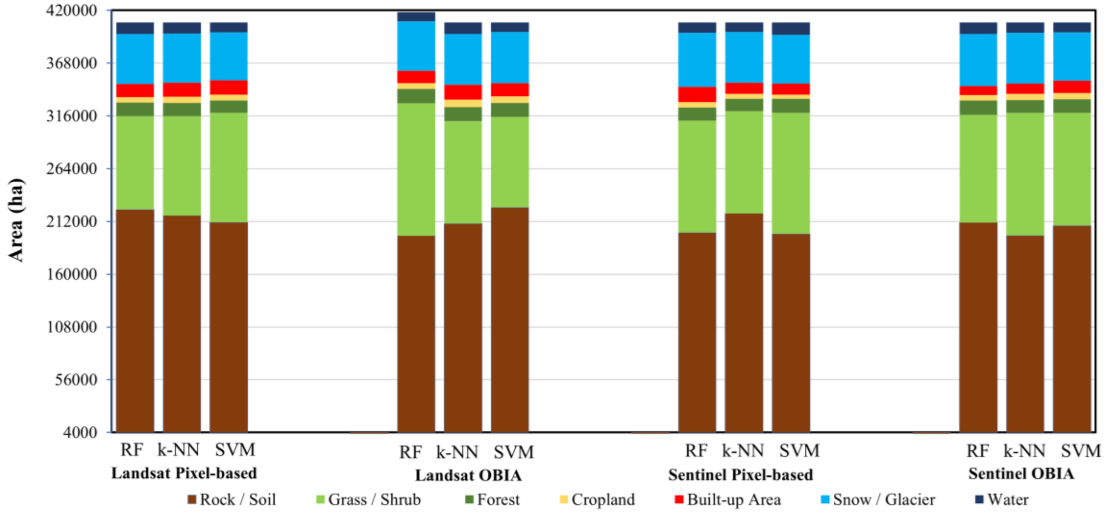

Figure 5. Area comparison of Land cover classes

Discussions:

In a pixel-based classification framework, RF consistently excelled the other two classifiers for both Landsat-8 and Sentinel-2 imagery. RF achieved the highest OA of 82.9% OA and a 0.796 Kappa coefficient, and an OA of 78% with a kappa coefficient of 0.737 on Sentinel-2. The superior performance of RF in pixel-based applications is probably due to its high stability and resistance to overfitting and noise, making it suitable for high-dimensional data sets [21]. SVM also showed reasonable results but lagged slightly behind RF. It performed well on Landsat-8 imagery by attaining 81.3% OA and 0.777 Kappa coefficient, but fell behind in performing with Sentinel-2 imagery, which may be due to the presence of mixed pixels and its sensitivity to spectral heterogeneity [18], k-NN produces lower accuracy, which is due to its reliance on distance metrics, which become less effective in heterogeneous landscapes, especially in mountainous regions [22].

Interestingly, in the OBIA, k-NN surpassed RF and SVM by gaining OA of 81.3% with a kappa coefficient of 0.777 when applied to Landsat-8 imagery. It demonstrates that the use of multiresolution segmentation enhances class boundaries, which in turn helps k-NN by reducing within-class spectral variability and enabling more coherent neighborhood-based classification [20]. Similarly, with Sentinel-2 imagery, k-NN produced the highest OA and kappa coefficient by achieving 83.6% and 0.80, respectively. RF and SVM showed decreased performance in object-based classification, especially with Sentinel-2, which is likely due to segment heterogeneity and mixed pixels resulting from high resolution [12], making it harder for RF and SVM to classify accurately.

In terms of land cover area distribution, SVM, despite having slightly lower accuracy in object-based classification, produced the most considerable extent of barren land in several instances, possibly due to its sensitivity to spectral variation and its tendency to overgeneralize spectrally similar classes [18]. RF demonstrated more balanced area allocation, which is evident in its strength in pixel-based classification [16]. An algorithm with high accuracy may not necessarily yield realistic area estimates if it over- or under classifies specific land cover types due to spectral confusion or lazy learning [20]. Additionally, the area among different land covers could change due to seasonal issues [26].

The comparative assessment of both classification methods using three ML classifiers on multi-resolution imagery provides a significant understanding and clear trends in the effectiveness of classifier behavior under varying spatial and spectral resolutions. Overall, the results exhibit that the classification method influences the classifier's performance. Pixel-based classification supports RF due to its strength in spectral analysis, while OBIA obliges k-NN due to the homogeneity of segmented objects.

However, our research has some limitations. The performance of classifiers was analyzed on default parameters without fine-tuning hyperparameters; segmentation parameters were selected manually, which may not be optimal across all landscapes. The study also focused on a single time frame (September), limiting the results across inter-annual variations and seasonality issues. Future research should consider integrating multi-temporal imagery with the use of topographic indices to enhance classification accuracy. The adoption of Deep Learning techniques or hybrid models could further improve classification results. An OBIA method using k-NN with high-resolution imagery is proposed for classification, incorporating multi-temporal analysis and automated parameter optimization for segmentation tuning to mitigate bias and enhance reproducibility.

Therefore, for complex mountainous areas like Gilgit District, choosing a suitable classification method and algorithm should align with the spatial and spectral resolutions of datasets and the specific goals of the analysis. OBIA approach using k-NN emerged as the best-performing combination overall, particularly with Sentinel-2, indicating it is optimal for high-resolution, spatially heterogeneous landscapes. These findings underscore the necessity of reliable LULC maps in practical applications such as environmental monitoring, disaster preparedness, and for accurate area estimation and planning.

Conclusion:

This study provides a comprehensive evaluation of pixel-based and OBIA classification approaches using three widely adopted ML classifiers, SVM, RF, and k-NN, under Landsat-8 and Sentinel-2 imagery for LULC mapping in the mountainous terrain of Gilgit District, Pakistan. This research demonstrates that classification performance is significantly dependent on the interaction between the spatial resolution of imagery, the segmentation method, and the classifier used. Pixel-based classification demonstrated the highest accuracy with RF, while k-NN obtained the highest accuracy in the OBIA method. Overall, the OBIA, combined with k-NN, applied to Sentinel-2 imagery, yields promising results.

The use of the above-mentioned techniques is recommended and should be adopted by the government to integrate land cover monitoring, support data-driven policies, promote sustainable land use, and facilitate climate-resilient development. This examination provides a solid foundation for helping in future land cover analysis and change detection efforts.

Acknowledgement:

We extend our sincere appreciation to the organizations and platforms that provided the geospatial resources utilized in this study. The freely accessible satellite imagery and processing capabilities offered by the Google Earth Engine (GEE) platform were instrumental in enabling large-scale data analysis. We also acknowledge the European Space Agency (ESA) Copernicus Programme for providing high-resolution Sentinel-2 data, and the United States Geological Survey (USGS) for managing the Landsat-8 product and also for making the SRTM Digital Elevation Model (DEM) openly available. Additionally, we thank Google for making Google Earth Pro available, which supported visual validation. The open access to these valuable datasets and platforms has significantly contributed to the success and reproducibility of this research.

Authors Contribution:

Conceptualization and supervision: Sawaid Abbas, formal analysis: Mati ur Rehman, Raja Tashfeen Muqarrab, methodology: Mati ur Rehman, writing—original draft preparation: Mati ur Rehman, Abdul Wahab Shah, writing—review and editing: Sawaid Abbas, Syed Aun Abbas, Dur E Najaf Raza, visualization: Mati ur Rehman. All authors have read and agreed to the published version of the manuscript.

Conflict of Interest: The authors declare no competing interests.

References:

[1] K. S. I. M. Z. Hasan, R. S. Leya, "Comparative Assessment of Machine Learning Algorithms for Land Use and Land Cover Classification Using Multispectral Remote Sensing Image," *Khulna Univ. Stud.*, pp. 33–46, doi: 10.53808/kus.2022.icstem4ir.0124-se.

[2] A. Jamali, "Evaluation and comparison of eight machine learning models in land use/land cover mapping using Landsat 8 OLI: a case study of the northern region of Iran," *SN Appl. Sci.*, vol. 1, no. 11, pp. 1–11, Nov. 2019, doi: 10.1007/S42452-019-1527-8/FIGURES/4.
[3] A. N. D. & E. Z. Hamidreza Khodaei, Farzin Nasiri Saleh, "Future flood susceptibility mapping under climate and land use change," *Sci. Rep.*, vol. 15, no. 12394, 2025, doi: https://doi.org/10.1038/s41598-025-97008-0.
[4] M. R. Haque, M. K. Tusar, M. A. Mou, and M. S. Rahaman, "Assessment of LULC change and its impact on Surface Runoff using SCS-CN method for Noakhali Region, Bangladesh," *Present Environ. Sustain. Dev.*, vol. 18, no. 1, pp. 277–292, 2024, doi: 10.47743/PESD2024181020.
[5] S. Aldiansyah and R. A. Saputra, "COMPARISON OF MACHINE LEARNING ALGORITHMS FOR LAND USE AND LAND COVER ANALYSIS USING GOOGLE EARTH ENGINE (CASE STUDY: WANGGU WATERSHED)," *Int. J. Remote Sens. Earth Sci.*, vol. 19, no. 2, pp. 197–210, Jan. 2023, doi: 10.30536/J.IJRESES.2022.V19.A3803.
[6] R. Saini and S. Singh, "Land use land cover mapping and snow cover detection in Himalayan region using machine learning and multispectral Sentinel-2 satellite imagery," *Int. J. Inf. Technol.*, vol. 16, no. 2, pp. 675–686, Feb. 2024, doi: 10.1007/S41870-023-01673-1/METRICS.
[7] L. Ghayour *et al.*, "Performance evaluation of sentinel-2 and landsat 8 OLI data for land cover/use classification using a comparison between machine learning algorithms," *Remote Sens.*, vol. 13, no. 7, p. 1349, Apr. 2021, doi: 10.3390/RS13071349/S1.
[8] G. H. Nitu Wu, Luís Guilherme Teixeira Crusiol, Guixiang Liu, Deji Wuyun, "Comparing Machine Learning Algorithms for Pixel/Object-Based Classifications of Semi-Arid Grassland in Northern China Using Multisource Medium Resolution Imageries," *Remote Sens*, vol. 15, no. 3, p. 750, 2023, doi: https://doi.org/10.3390/rs15030750.
[9] L. W. L. Thanh Noi Phan, Verena Kuch, "Land Cover Classification using Google Earth Engine and Random Forest Classifier—The Role of Image Composition," *Remote Sens*, vol. 12, no. 15, p. 2411, 2020, doi: https://doi.org/10.3390/rs12152411.
[10] J. S. Zhaobin Wang, Yikun Ma, Yaonan Zhang, "Review of Remote Sensing Applications in Grassland Monitoring," *Remote Sens*, vol. 14, no. 12, p. 2903, 2022, doi: https://doi.org/10.3390/rs14122903.
[11] Y. E. Ş. Mustafa Özbuldu, "Comparative analysis of different supervised methods for satellite-based land-use classification: A case study of Reyhanlı," *Mustafa Kemal Univ. J. Agric. Sci.*, vol. 29, no. 3, p. 12, 2024, doi: https://doi.org/10.37908/mkutbd.1485236.
[12] N. Aggarwal, M. srivastava, and M. Dutta, "Comparative Analysis of Pixel-Based and Object-Based Classification of High Resolution Remote Sensing Images – A Review," *Int. J. Eng. Trends Technol.*, vol. 38, no. 1, pp. 5–11, Aug. 2016, doi: 10.14445/22315381/IJETT-V38P202.
[13] Nishant Mehra & Janaki Ballav Swain, "Assessment of land use land cover change and its effects using artificial neural network-based cellular automation," *J. Eng. Appl. Sci.*, vol. 71, no. 70, 2024, doi: https://doi.org/10.1186/s44147-024-00402-0.
[14] A. Kumar, G. Kumar, D. S. Patil, and R. Gupta, "Evaluating Machine Learning Classifiers for IRS High Resolution Satellite Images Using Object-Based and Pixel-Based Classification Techniques," *J. Indian Soc. Remote Sens.*, vol. 53, no. 6, pp. 1799–1818, Jun. 2025, doi: 10.1007/S12524-024-02084-W/METRICS.
[15] H. . B. Gupta, Neha, "Object based Information Extraction from High Resolution Satellite Imagery using eCognition," *IJCSI Int. J. Comput. Sci. Issues*, vol. 11, no. 3, p. 2,

2014, [Online]. Available: https://ijcsi.org/papers/IJCSI-11-3-2-139-144.pdf
[16] M. I. S. & M. N. Gomal Amin, Iqra Imtiaz, Ehsan Haroon, Najum us Saqib, "Assessment of Machine Learning Algorithms for Land Cover Classification in a Complex Mountainous Landscape," *J. Geovisualization Spat. Anal.*, vol. 8, no. 34, 2024, doi: https://doi.org/10.1007/s41651-024-00195-z.
[17] S. R. Zohaib, N. Habib, A. Talha Manzoor, S. Abbas, "Comparative Assessment of Classification Algorithms for Land Cover Mapping Using Multispectral and PCA Images of Landsat," *Int. J. Innov. Sci. Technol*, vol. 6, no. 6, pp. 225–239, 2024, doi: https://journal.50sea.com/index.php/IJIST/article/view/840.
[18] Z.-Q. S. Ling-Min He, Fan-Sheng Kong, "Multiclass SVM based land cover classification with multisource data," *IEEE Xplore*, 2005, doi: 10.1109/ICMLC.2005.1527555.
[19] G. Guo, H. Wang, D. Bell, Y. Bi, and K. Greer, "KNN Model-Based Approach in Classification," *Lect. Notes Comput. Sci. (including Subser. Lect. Notes Artif. Intell. Lect. Notes Bioinformatics)*, vol. 2888, pp. 986–996, 2003, doi: 10.1007/978-3-540-39964-3_62.
[20] M. A. M. & E. G. Shahadat Uddin, Ibtisham Haque, Haohui Lu, "Comparative performance analysis of K-nearest neighbour (KNN) algorithm and its different variants for disease prediction," *Sci. Rep.*, vol. 12, no. 6256, 2022, doi: https://doi.org/10.1038/s41598-022-10358-x.
[21] M. Belgiu and L. Drăgu, "Random forest in remote sensing: A review of applications and future directions," *ISPRS J. Photogramm. Remote Sens.*, vol. 114, pp. 24–31, Apr. 2016, doi: 10.1016/J.ISPRSJPRS.2016.01.011.
[22] P. Thanh Noi and M. Kappas, "Comparison of Random Forest, k-Nearest Neighbor, and Support Vector Machine Classifiers for Land Cover Classification Using Sentinel-2 Imagery," *Sensors 2018, Vol. 18, Page 18*, vol. 18, no. 1, p. 18, Dec. 2017, doi: 10.3390/S18010018.
[23] Y. G. Shuai Xie, Liangyun Liu, Xiao Zhang, Jiangning Yang, Xidong Chen, "Automatic Land-Cover Mapping using Landsat Time-Series Data based on Google Earth Engine," *Remote Sens*, vol. 11, no. 24, p. 3023, 2019, doi: https://doi.org/10.3390/rs11243023.
[24] N. Gorelick, M. Hancher, M. Dixon, S. Ilyushchenko, D. Thau, and R. Moore, "Google Earth Engine: Planetary-scale geospatial analysis for everyone," *Remote Sens. Environ.*, vol. 202, pp. 18–27, Dec. 2017, doi: 10.1016/J.RSE.2017.06.031.
[25] L. C. Nadeem Ullah, "Insights into climate change dynamics: A tourism climate index-based evaluation of Gilgit-Baltistan, Pakistan," *Heliyon*, vol. 10, no. 15, p. e35315, 2024, [Online]. Available: https://www.cell.com/heliyon/fulltext/S2405-8440(24)11346-1?_returnURL=https%3A%2F%2Flinkinghub.elsevier.com%2Fretrieve%2Fpii%2FS2405844024113461%3Fshowall%3Dtrue
[26] A. Q. B. Amjad Ali Khan, Xian Xue, Hassam Hussain, Kiramat Hussain, Ali Muhammad, Muhammad Ahsan Mukhtar, "Study of Land Surface Changes in Highland Environments for the Sustainable Management of the Mountainous Region in Gilgit-Baltistan, Pakistan," *Sustainability*, vol. 16, no. 23, p. 10311, 2024, doi: https://doi.org/10.3390/su162310311.
[27] "Birds of Gilgit-Baltistan - Home." Accessed: Jul. 23, 2025. [Online]. Available: https://www.birdsofgilgit.com/index.html
[28] "Landsat 8 | U.S. Geological Survey." Accessed: Jul. 23, 2025. [Online]. Available: https://www.usgs.gov/landsat-missions/landsat-8
[29] F. G. Osman Salih Yilmaz, "Chapter 9 - Investigation of surface water dynamics from the Landsat series using Google Earth Engine: A case study of Lake Bafa," *Google Earth Engine Artif. Intell. Earth Obs.*, pp. 177–193, 2025, doi: https://doi.org/10.1016/B978-0-443-27372-8.00013-1.

[30] C. Martin Claverie, Junchang Ju, Jeffrey G. Masek, Jennifer L. Dungan, Eric F. Vermote, Jean-Claude Roger, Sergii V. Skakun, Justice, "The Harmonized Landsat and Sentinel-2 surface reflectance data set," *Remote Sens. Environ.*, vol. 219, pp. 145–161, 2018, doi: https://doi.org/10.1016/j.rse.2018.09.002.

[31] S. A. S. Siti Aminah Anshah, Nurul Ain Nabilah Sharuddin, "Chapter 24 - Mature and immature oil palm classification from image Sentinel-2 using Google earth engine (GEE)," *Google Earth Engine Artif. Intell. Earth Obs.*, pp. 465–487, 2025, doi: https://doi.org/10.1016/B978-0-443-27372-8.00001-5.

[32] Sudhir K. Powar, "An Evaluation of Pixel-based and Object-based Classification Methods for Land Use Land Cover Analysis Using Geoinformatic Techniques," *Geomatics Environ. Eng.*, vol. 16, no. 2, p. 2, 2022, [Online]. Available: https://www.gaee.agh.edu.pl/gaee/article/view/182

[33] H. R. El Mehdi Sellami, "A NEW APPROACH FOR MAPPING LAND USE / LAND COVER USING GOOGLE EARTH ENGINE: A COMPARISON OF COMPOSITION IMAGES," *Int. Arch. Photogramm. Remote Sens. Spat. Inf. Sci.*, 2023, [Online]. Available: https://isprs-archives.copernicus.org/articles/XLVIII-4-W6-2022/343/2023/

[34] J. A. & J. C. Zhiwen Li, Xingyu Chen, Jie Qi, Chong Xu, "Accuracy assessment of land cover products in China from 2000 to 2020," *Sci. Rep.*, vol. 13, no. 12936, 2023, doi: https://doi.org/10.1038/s41598-023-39963-0.

[35] M. C. Cidália C. Fonte, Diogo Duarte, Ismael Jesus, Hugo Costa, Pedro Benevides, Francisco Moreira, "Accuracy Assessment and Comparison of National, European and Global Land Use Land Cover Maps at the National Scale—Case Study: Portugal," *Remote Sens*, vol. 16, no. 9, p. 1504, 2024, doi: https://doi.org/10.3390/rs16091504.